



1 Streamflow indices to identify catchment drivers of 2 hydrograph

3 Jeenu Mathai¹ and Pradeep P. Mujumdar^{1,2}

4 ¹Department of Civil Engineering, Indian Institute of Science, Bangalore, India

5 ²Interdisciplinary Centre for Water Research, Indian Institute of Science, Bangalore, India

6 Correspondence to: P. P. Mujumdar (pradeep@iisc.ac.in)

7

8 **Abstract.** Streamflow indices are flow descriptors that quantify the streamflow dynamics, which are usually
9 determined for a specific basin and are distinct from other basin features. The flow descriptors are appropriate for
10 large-scale and comparative hydrology studies, independent of statistical assumptions and can distinguish signals
11 that indicate basin behavior over time. In this paper, the characteristic features of the hydrograph's temporal
12 asymmetry due to its different underlying hydrologic processes are primarily highlighted. Streamflow indices
13 linked to each limb of the hydrograph within the time-irreversibility paradigm are distinguished with respect to
14 its processes driving the rising and falling limb. Various streamflow indices relating the rising and falling limbs,
15 and the catchment attributes such as climate, topography, vegetation, geology and soil are then correlated. Finally,
16 the key attributes governing rising and falling limbs are identified. The novelty of the work is on differentiating
17 hydrographs by their time irreversibility property and offering an alternative way to recognize primary drivers of
18 streamflow hydrographs. A set of streamflow indices at the catchment scale for 671 basins in the Contiguous
19 United States (CONUS) is presented here. These streamflow indices complement the catchment attributes
20 provided earlier (Addor et al., 2017) for the CAMELS data set. A series of spatial maps describing the streamflow
21 indices and their regional variability over the CONUS is illustrated in this study.

22

23 1 Introduction

24 Hydrologists use data to underpin the hydrologic system by identifying several unique catchment signatures and
25 employ various flow descriptors independent of statistical assumptions yet capable of capturing signals that reflect
26 the basin's long-term unique behavior. Hydrological indices, commonly referred to as hydrologic metrics,
27 hydrologic signatures, or diagnostic signatures, are quantitative flow metrics that characterize statistical or
28 dynamical hydrological data series (McMillan, 2021). Specifically, streamflow indices are flow descriptors
29 derived from discharge time-series data, and a considerable collection of indices are available to aid in the better
30 characterization of hydrological features, ranging from basic statistics like the mean to more sophisticated metrics
31 (Addor et al., 2018; McMillan, 2021). In many cases, daily streamflow records are not permitted for redistribution;
32 however, researchers have computed streamflow indices and made them publicly accessible.

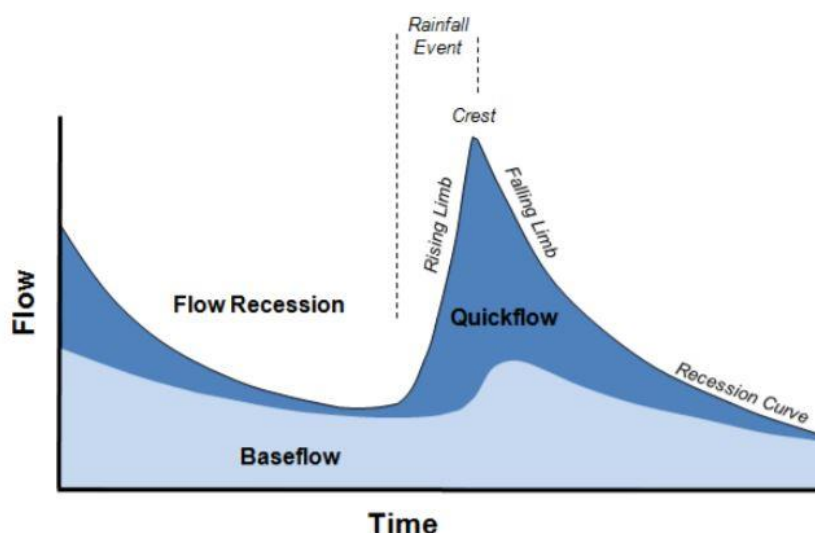
33

34 Hydrological indices are increasingly used in emerging areas such as global-scale hydrologic modeling and large-
35 sample hydrology to extract relevant information and compare the different watershed processes (Addor et al.,
36 2017, 2018; McMillan, 2021). These indices offer an indirect way to explore hydrological processes as well as
37 provide insights into hydrologic behavior in catchments where data other than streamflow is restricted and are



38 widely used in process exploration, model calibration, model selection, and catchment classification (Addor et al.,
 39 2018; Clark et al., 2011; Kuentz et al., 2017; McMillan et al., 2011; Sawicz et al., 2011). McMillan (2021)
 40 presented a classification that differentiates between statistics- and dynamics-based signatures and between
 41 signatures at different timescales.

42
 43 The relevance of time irreversibility (or temporal asymmetry) of streamflow variability on a daily scale has been
 44 emphasized in recent studies (Koutsoyiannis, 2020; Mathai and Mujumdar, 2019; Serinaldi and Kilsby, 2016) the
 45 disparity in physical mechanisms driving the hydrograph's ascension and recession limbs (Fig.1) contributes to
 46 time irreversibility. Unlike other variables such as temperature, wind, precipitation, time irreversibility has been
 47 marked for streamflow at a daily scale (Koutsoyiannis, 2020). Moreover, the various segments of the recession
 48 phase represent different phases in the flow process. As a result, time irreversibility must be acknowledged in
 49 streamflow analysis, accounting for the distinction of the recession into different segments, with a faster recession
 50 induced by high discharges caused by surface runoff and a slower recession caused by baseflow (Fig.1), and the
 51 characterization of the recession rates separately (Mathai and Mujumdar, 2019). In this study, streamflow indices
 52 are chosen to better understand different hydrological processes by recognizing the streamflow hydrograph's
 53 temporal asymmetry.



55
 56 **Figure 1.** Schematic representation of rising limb and falling limb
 57 (source: Environment Southland;
 58 <https://www.es.govt.nz/environment/water/groundwater/groundwater-monitoring>)

59 60 2 Methods

61 To facilitate a comprehension of various hydrological processes and streamflow hydrograph drivers, the study
 62 employs streamflow indices considering the streamflow hydrograph's temporal asymmetry. The description of
 63 indices used in this study are tabulated in Table 1. Streamflow indices linked to each limb of the streamflow
 64 hydrograph within the time-irreversibility paradigm are distinguished since hydrographs have rising and falling



limbs. The following indices are considered in the rising limb category: 1) rising limb density, 2) rising limb shape parameter, and 3) rising limb scale parameter. In contrast, 1) falling limb density 2) slope of upper recession (upper recession coefficient) 3) slope of lower recession (lower recession coefficient) are selected in falling limb category. The next step is to compute these indices for a large number of catchments and correlate them with attributes such as climate, topography, vegetation, geology, and soil. The streamflow indices can be correlated explicitly since sub-categories are involved in each of the catchment attributes discussed above. Finally, the key attributes governing ascension and recession limbs can be summarized and identified. This work's main novelty is to differentiate hydrographs by their time irreversibility property and using their associated indices by offering an alternative way to recognize primary drivers of streamflow hydrographs. The specifics of indices are explained further below.

Rising limb density (RLD) is defined as the ratio of the number of rising limbs and the cumulative time of rising limbs (Shamir et al., 2005). RLD is a hydrograph shape descriptor without considering the flow magnitude (Fig. 2) and the expression for RLD is given as,

$$RLD = \frac{N_r}{T_r} \quad (1)$$

The ratio of the number of falling limbs to the cumulative time of falling limbs is termed as falling limb density (FLD) (Fig. 2) (Shamir et al., 2005). The expression for FLD is given as,

$$FLD = \frac{N_{FL}}{T_F} \quad (2)$$

Table 1. Hydrological descriptors with temporal asymmetry.

Sl.no	Attribute	Description	Unit	Data source	References
1	RLD	Rising limb density	day ⁻¹	N15 – USGS data	Shamir et al. (2005)
2	FLD	Falling limb density	day ⁻¹		
3	a	ascension limb scale parameter	-		Mathai and Mujumdar, (2019)
4	b	ascension limb shape parameter	-		
5	b ₁	Upper recession coefficient	-		
6	b ₂	Lower recession coefficient	-		

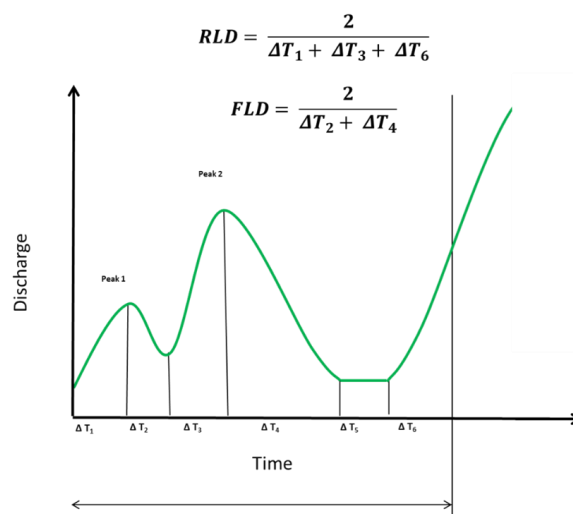


Figure 2. Schematic example of rising limb density (RLD) and falling limb density (FLD) calculation (Shamir et al., 2005).

The diurnal increments of streamflow are fitted with an appropriate probability density function to depict the shape of the ascension limbs which occur on wet days. The Weibull distribution reflects the diurnal increments of streamflow that occur on wet days reasonably well (Mathai and Mujumdar, 2019; Stagge and Moglen, 2013; Szilagyi et al., 2006), and the scale 'a' and shape 'b' parameters of the Weibull distribution are computed for each catchment by using observed diurnal increments of streamflow. In contrast, an exponential recession is used to capture the shape of the recession limbs on dry days of the daily hydrograph, representing the falling limbs' underlying dynamics (Mathai and Mujumdar, 2019). As the upper recession refers to the fast flow following a storm event and the lower recession refers to the baseflow recession, falling limb modeling is done in two stages.

The study uses indices related to ascension limb (viz., RLD, ascension limb scale parameter, ascension limb shape parameter) and recession limb (viz., FLD, upper recession coefficient, lower recession coefficient) to summarize the characteristic shape of steeper rising and gradually declining falling limb and its application in understanding the role of various drivers of catchment attributes in streamflow generation.

3 Contributions of the Study

The analysis employs a collection of indices drawn from hydrograph shape diagnoses, which extracts information about a basin's ascension and recession limbs' inherent properties. The principle of time irreversibility is encapsulated by six streamflow indices that describe and characterize a streamflow hydrograph's shape, and indices for a particular basin are consistent and distinct from indices from other basins.



105 The goals of this study are as follows: i) to identify the key drivers of streamflow hydrographs (in terms
 106 of catchment attributes) using time-irreversibility-based indices ii) to present a spatial map-based attribute
 107 class of time-irreversibility-based indices for a large sample hydrology dataset.

108 As shown in numerous ways/studies in the literature, our notion of time-irreversibility and its indices
 109 could also do a reasonable job of articulating the catchment drivers of streamflow hydrographs. This
 110 study presents an attribute class of hydrograph shape descriptors with temporal asymmetry. The
 111 significance of large sample hydrology datasets in open hydrologic science and their potential to improve
 112 hydrological studies' transparency is also underlined in this study.

113 **4 Motivation to extend to large sample hydrology**

114 Large-sample hydrology (LSH) gathers information from a larger number of catchments to gain a more
 115 comprehensive understanding of hydrological processes and to go beyond individual case studies. LSH
 116 helps identify catchment behavior and leads one to derive precise conclusions regarding different
 117 hydrological processes and models (Addor et al., 2020). Studies involving large sample catchments help
 118 in understanding the drivers of hydrological change (Blöschl et al., 2019), in assessing hydrological
 119 similarity and classification (Berghuijs et al., 2014; K. A. Sawicz et al., 2014), in predictions in ungauged
 120 basins (Ehret et al., 2014), and in analysing model and data uncertainty (G. Coxon et al., 2014) and foster
 121 hydrology research by standardizing and automating the creation of large sample hydrology datasets
 122 worldwide (Addor et al., 2020). LSH assists in exploring interrelationships between numerous catchment
 123 attributes related to landscape, climate, and hydrology (Addor et al., 2017; Alvarez-Garreton et al., 2018;
 124 Gupta et al., 2014; Newman et al., 2015; K. Sawicz et al., 2011) and generalizing rules that can
 125 significantly improve the predictability of the water cycle (Alvarez-Garreton et al., 2018).

126 The primary challenges in fostering LSH are data availability and accessibility, which seriously hinder
 127 its use in data-scarce regions. Despite the fact that a few large-scale hydrology studies have been
 128 undertaken, the number of publicly available large-scale datasets is still restricted (Addor et al., 2017,
 129 2020; Coxon et al., 2020). Moreover, licensing restrictions and strict access policies make the datasets
 130 rarely available to the public (Coxon et al., 2020).

131 Model Parameter Estimation Experiment project (MOPEX) dataset (Duan et al., 2006), Canadian model
 132 parameter experiment (CANOPEX) database (Arsenault et al., 2016), Global Streamflow Indices and
 133 Metadata Archive (Do et al., 2018; Gudmundsson et al., 2018), Global Runoff Reconstruction (Ghiggi et
 134 al., 2019), HydroATLAS (Linke et al., 2019) and the Catchment Attributes and MEteorology for Large-
 135 Sample studies (CAMELS) (Addor et al., 2017) are notable contributions of open and accessible large
 136 sample catchment datasets (Coxon et al., 2020).

137 Addor et al. (2017) introduced a new dataset (CAMELS) made publicly available for large-sample
 138 hydrological studies. This dataset covers meteorological and streamflow datasets provided by Newman
 139 et al. (2015) and provides quantitative metrics for a large variety of attributes for 671 catchments in the
 140 contiguous United States (CONUS). Streamflow records are available in the dataset from 1990 to 2009
 141 for the 671 catchments, which are minimally influenced by human activities (Addor et al., 2017).



142 The CAMELS dataset prompted hydrological research by enabling open access to hydrologic data and
 143 establishing a common standard across the database. CAMELS promoted open access to datasets for the
 144 United States, and it is eventually expanded to the United Kingdom (CAMELS-GB), Chile (CAMELS-
 145 CL), and Brazil (CAMELS-BR). The CAMELS proposes five classes of catchment attributes, namely
 146 location, topography, geology, land cover characteristics, climatic indices, and hydrological signatures,
 147 in order to promote common standards and formats in large sample studies (Addor et al., 2017). The
 148 concept of time irreversibility-based streamflow indices is then applied to CAMELS catchments with the
 149 goal of encouraging large sample hydrology studies.

150 **5 Dataset used**

151 Section 5 provides the description of the dataset used and the study area chosen. This study employs the
 152 CAMELS dataset, which encompasses daily discharge data and catchment attributes for 671 catchments
 153 (Fig. 3) across the continental United States, representing a diverse set of catchments with long
 154 streamflow time series covering a wide range of hydro-climatic conditions (Addor et al., 2017). The time
 155 frame chosen for the analysis is from 1 October 1989 to 30 September 2009 (Addor et al., 2017). The
 156 topographic characteristics of CAMELS dataset are represented in Fig. 4. Except for the Appalachian
 157 Mountains, the eastern part of the Continental United States is much flatter than the western portion,
 158 according to mean elevation and mean slope maps (Fig. 4.a and 4.b). Figure 4.c depicts the spatial pattern
 159 of catchment size, highlighting presence of some catchments with an area greater than 10,000 km².

160

161

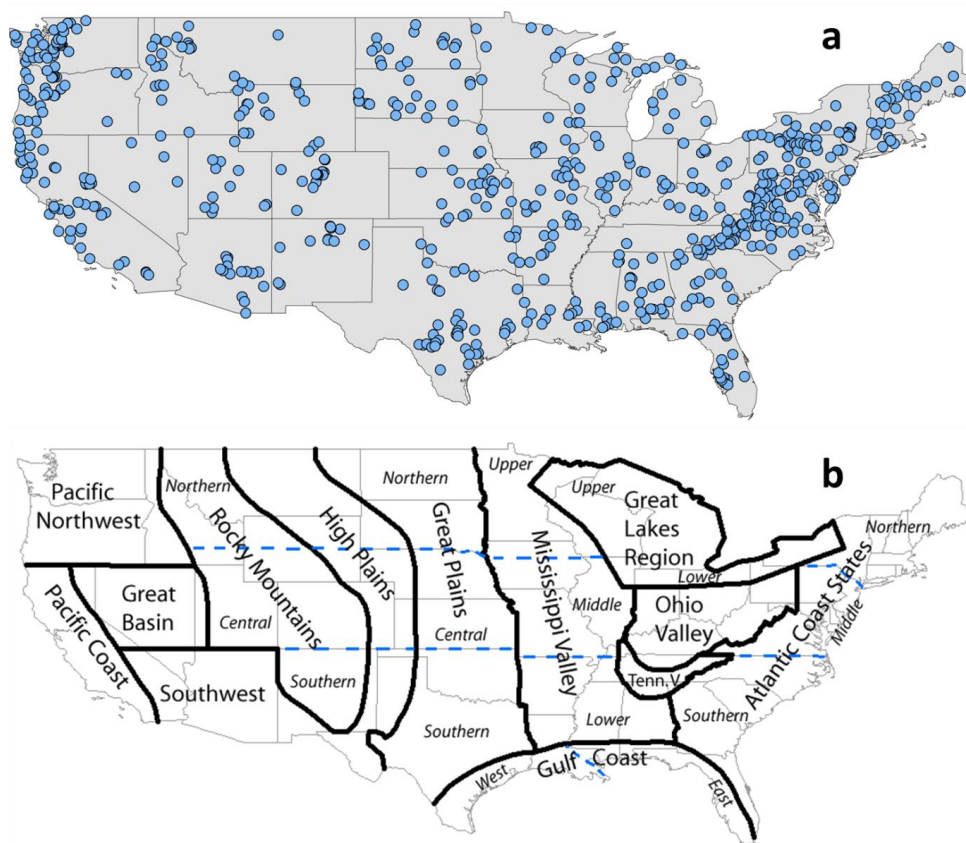


Figure 3. (a) Map of 671 CAMELS catchments in the continental United States considered in this study.
 (b) Geographical regions of US according to NOAA National Centers for Environmental Information
 referred for the analysis (source: NOAA National Centers for Environmental Information;
<https://www.ncdc.noaa.gov/temp-and-precip/drought/nadm/geography>).

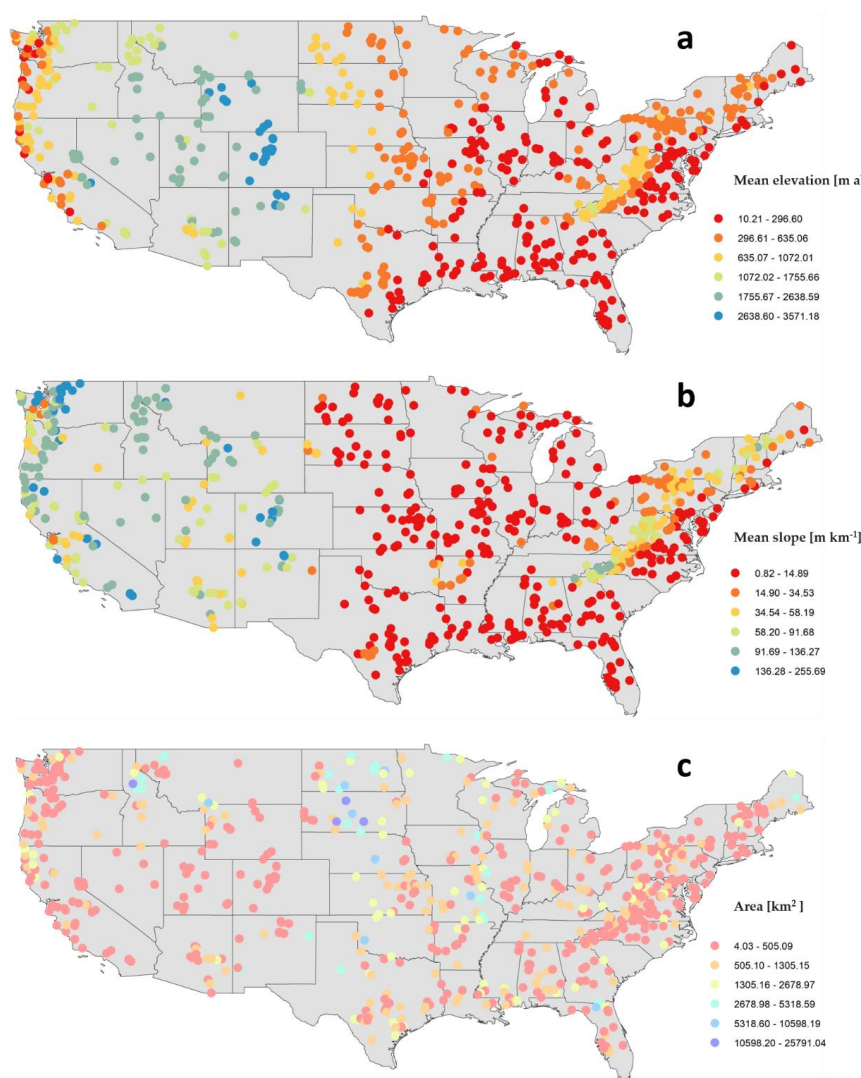


Figure 4. Maps of topographic characteristics of CAMELS catchments over the CONUS (Addor et al., 2017). (a) Mean elevation [m above sea level] (b) Mean slope [m km⁻¹] (c) Area [km²]. The eastern US seems to have a much flatter mean elevation and mean slope than the western US, which significantly influences catchment behavior. The majority of the catchments are noticed to be smaller, with an area of fewer than 3000 km².



5.1 Catchment attributes

The landscape of each catchment is described using multiple attributes, which can be divided into various classes as shown in Table 2 (Addor et al., 2017). The details of the attributes used in this study is summarized in Table 2.

Table 2. CAMELS attributes (Addor et al., 2017)

Sl.no	Attribute	Description	Unit
Climatic indices			
1	aridity	aridity (ratio of mean PET to mean precipitation)	-
2	p_seasonality	seasonality and timing of precipitation (positive (negative) values indicate that precipitation peaks in summer (winter); values close to 0 indicate uniform precipitation throughout the year)	-
3	frac_snow	fraction of precipitation falling as snow	-
4	high_prec_freq	frequency of high precipitation days	days yr ⁻¹
5	high_prec_dur	average duration of high precipitation events	days
6	low_prec_freq	frequency of dry days	days yr ⁻¹
7	low_prec_dur	average duration of dry periods	days
Land cover characteristics			
8	Forest_frac	forest fraction	-
9	Lai_max	maximum monthly mean of the leaf area index	-
10	Gvf_max	maximum monthly mean of the green vegetation fraction	-
Soil characteristics			
11	soil_depth_pelletier	depth to bedrock	m
12	sand_frac	sand fraction	%
13	clay_frac	clay fraction	%
Geological characteristics			
14	geol_porosity	subsurface porosity	-
15	geol_permeability	subsurface permeability (log10)	m ²



196 6 Results and Discussion

197 The first sub-section below looks at the regional variability of the streamflow indices used in this study. For the
 198 671 CAMELS catchments, rising limb density, falling limb density, ascension limb scale parameter, ascension
 199 limb shape parameter, upper recession coefficient, and lower recession coefficient are computed and given as
 200 spatial maps. Streamflow indices are then presented in hydrological clusters to incorporate a more explicit spatial
 201 representation of catchment behavior across the CONUS. Catchment attributes cover a broad range of aspects of
 202 catchment hydrology such as, land cover, soil, climate, geology, topography and the association between these
 203 attributes and streamflow indices is discussed further in the subsequent section. As the climate is the most
 204 important factor in the US for the hydrological behavior for the CAMELS dataset (Jehn et al., 2020), the influence
 205 of climatic factors on streamflow indices is finally studied.







206 6.1 Spatial Variability in Streamflow Indices

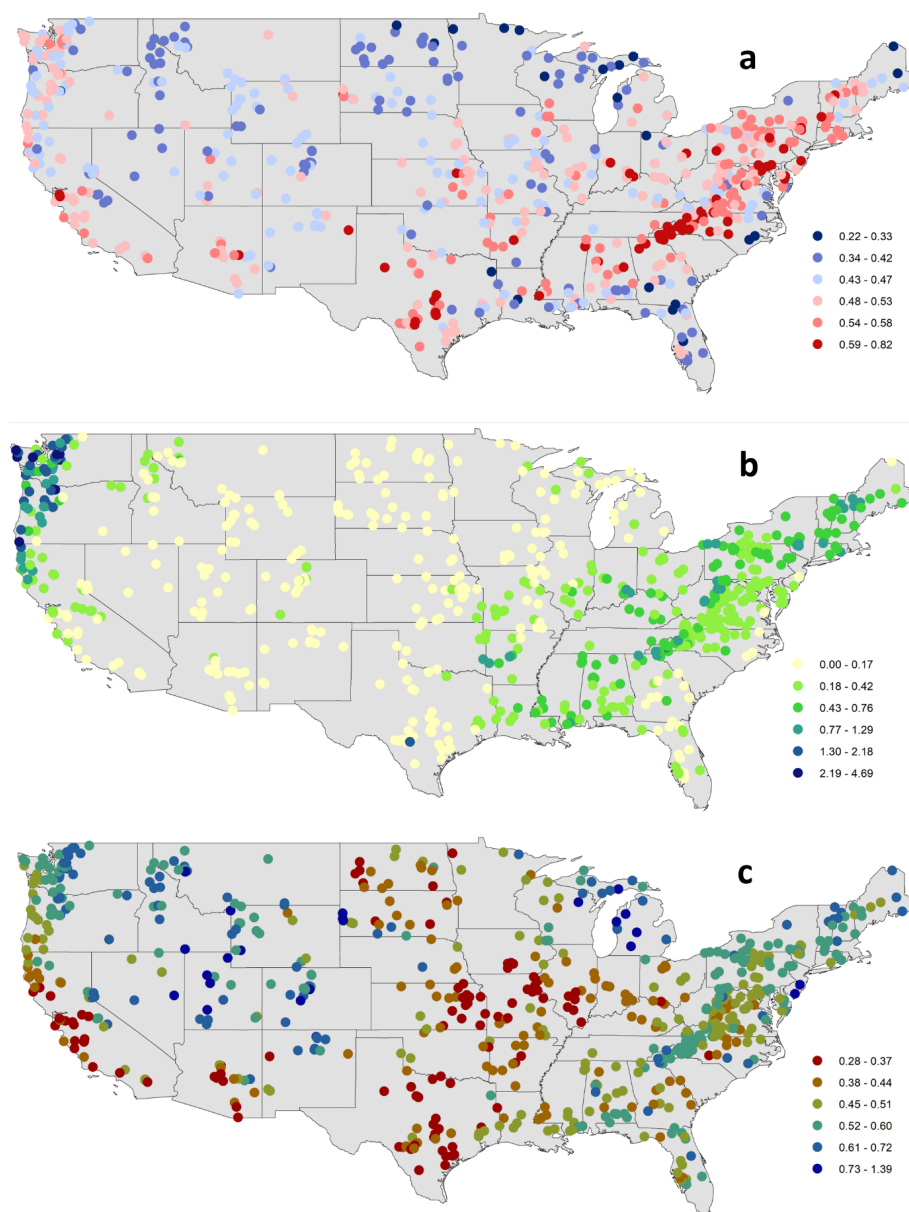
207 Streamflow indices related to rising limbs and falling limbs are computed for the selected catchments and
 208 displayed in spatial maps as shown in Fig. 5 and Fig. 6, respectively. The spatial analysis is based on the United
 209 States' geographical areas (for details, refer to Fig. 3b) as defined by NOAA's National Centers for Environmental
 210 Information and is referred to in the following spatial maps. Furthermore, ten clusters provided by Jehn et al.
 211 (2020) to represent the discrete hydrological behaviors of the continental United States are adopted in this study
 212 to understand the regional variability of catchment behavior. Figure S1 and Table S1 present the location map and
 213 details of the ten clusters.

214 In terms of geographical regions, the rising limb density is highest over the Atlantic coast states, Ohio valley,
 215 Lower Mississippi Valley, Southern Great Plains, Southwest and Pacific, and lowest along the Upper Great Lakes
 216 region, Upper Mississippi Valley, Great Basin, and Northern Rocky Mountains, Northern Interior Plains, and East
 217 of Gulf Coast (Fig. 5.a). Further, in terms of hydrological clusters, Appalachian Mountains (Cluster 10),
 218 Southeastern and Central Plains (Cluster 1) and all Southern most states of the US (Cluster 9) witness high rising
 219 limb densities and these clusters are characterized by a high forest fraction, low aridity, and high frequency of
 220 high precipitation events, respectively (Fig. 6.a). Northwestern Forested Mountains (Clusters 3, 4), located in the
 221 mountains of the western US, experience low values of rising limb density as these clusters are characterized by
 222 a dominant summer peak of discharge caused by rapid snowmelt (Fig. 6.a).

223 Considerably low values of rising limb scale parameters are experienced over the Rocky Mountains, High Plains,
 224 Great Plains, Upper Mississippi Valley, Great Basin, Southwest, and the Great Lakes regions, whereas the Pacific
 225 Northwest shows high values of rising limb scale parameters (Fig. 5.b). Clusters (5, 7) over the Northwestern
 226 Forested Mountains of CONUS experience very high values of rising limb scale parameters (Fig. 6.b). These
 227 catchments have the highest discharge, especially in the early summer, due to a combination of high precipitation
 228 and snowmelt. Further, the region in the Continental US which receives the highest precipitation is included in
 229 Cluster 5. Moreover, Cluster 5 consists of a large proportion of forest. Again, Cluster 7 with high values of rising
 230 limb scale parameter is characterized by high fraction of precipitation falling as snow. Low values of rising limb
 231 scale parameters are shown by Clusters 2, 8, 9. This is because of low water availability, low snow fraction
 232 precipitation falling as snow, and high evaporation experienced in these regions.



233 Low rising limb shape parameter occurs along the Great Plains, Mississippi Valley, Pacific coast, and the west of
 234 Gulf Coast (Fig. 5.c). In contrast, the shape parameter over the Rocky Mountains, High Plains, Great Basin, Pacific
 235 Northwest, and the Great Lakes region witnesses the highest values of rising limb shape parameters (Fig. 5.c). All
 236 the catchments located in the Southern states of the US (Cluster 9), Great Plains and North American deserts
 237 (Cluster 8), and the Central Plains (Cluster 2) characterize low values of rising limb shape parameters (Fig. 6.c).
 238  This is due to low water availability, low snow fraction precipitation falling as snow, low leaf area index, and high
 240  evaporation experienced in these regions. High values of rising limb shape parameters are seen in Clusters 3, 4
 241  (Fig. 6.c) located in the Northwestern Forested Mountains of the western US, dominant with a summer peak of
 242 discharge caused by rapid snowmelt.
 243 Catchments with a high falling limb density are predominantly located along the Great Basin and the Rocky
 244 Mountains and in the High Plains region (Fig. 7.a). Clusters 4, 2, 8 over Northwestern Forested Mountains, Central
 245 Plains, Great Plains, and North American deserts characterize higher magnitudes of falling limb density, and
 246 Clusters 6, 7 over Marine West Coast Forests and Western Cordillera smaller falling limb densities (Fig. 8.a).
 247  This is due to less presence of forest cover in these arid regions.
 248 Similarities exist between the patterns of the upper recession coefficient and the lower recession coefficient (Fig.
 249 7.b and Fig. 7.c). Clusters 3, 4 located in the Northwestern Forested Mountains, which have overall low discharge,
 250  show low values of upper and lower recession coefficients (Fig. 8.b and Fig.  Clusters 2, 9, located in the
 eastern US, witness high values of recession coefficients; due to low slope inclinations, water takes a long time
 to reach the outlet (Fig. 8.b and Fig. 8.c).

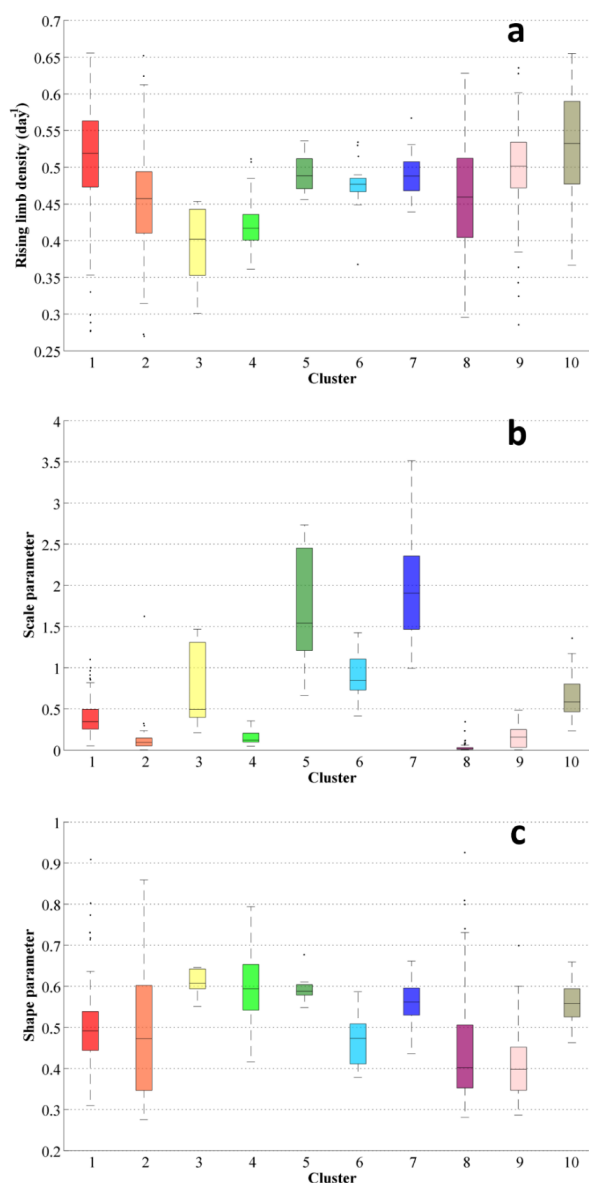


252

253 **Figure 5.** Spatial maps of streamflow indices associated with a rising limb (a) rising limb density [day⁻¹], (b)
 254 rising limb scale parameter, (c) rising limb shape parameter over the CONUS. The Atlantic coast states, Ohio
 255 Valley, Lower Mississippi Valley, Southern Great Plains, Southwest, and Pacific have the highest rising limb
 256 density, while the Upper Great Lakes region, Upper Mississippi Valley, Great Basin, Northern Rocky Mountains,
 257 Northern Interior Plains, and East of Gulf Coast have the lowest. The Rocky Mountains, High Plains, Great Plains,
 258 Upper Mississippi Valley, Great Basin, Southwest, and Great Lakes regions have low values of rising limb scale
 259 parameters, but the Pacific Northwest has high values of rising limb scale parameters. The Great Plains,
 260 Mississippi Valley, Pacific coast, and west of Gulf Coast have low rising limb shape parameters. The shape
 261 parameter has the greatest values of rising limb shape parameters over the Rocky Mountains, High Plains, Great
 262 Basin, Pacific Northwest, and Great Lakes regions.



263

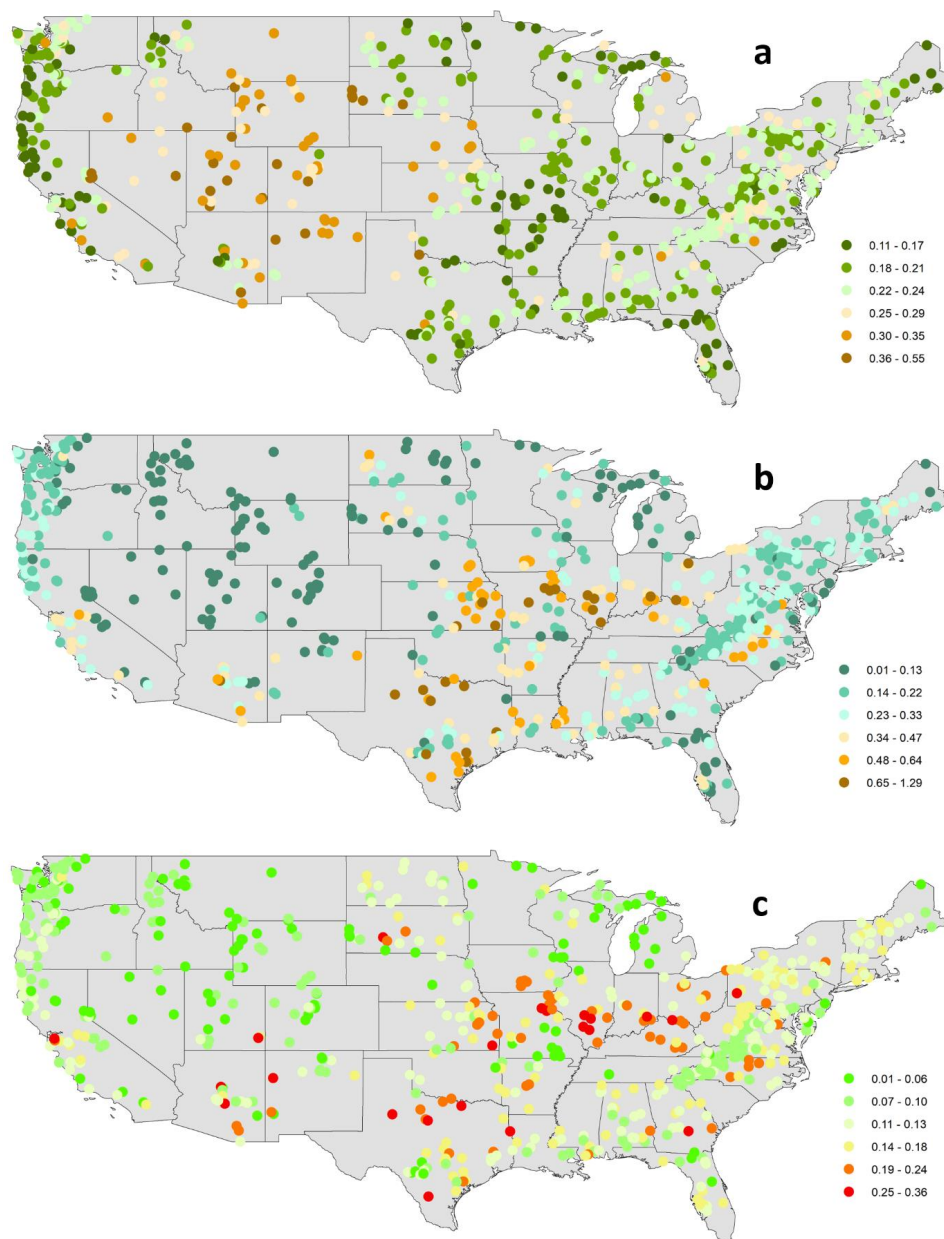


264

Figure 6. Boxplots of the hydrological descriptors linked with the rising limb (a) rising limb density [day^{-1}], (b) rising limb scale parameter, (c) rising limb shape parameter of the clusters over the CONUS. High rising limb densities are observed in Clusters 10, 1, and 9, which are characterized by a high forest fraction, low aridity, and a high frequency of high precipitation events, respectively. Rising limb scale parameters are exceptionally high in Clusters 5, 7. Due to a combination of high precipitation and snowmelt, these catchments have the highest discharge. Because of the low water availability, low snow fraction precipitation falling as snow, low leaf area index, and high evaporation experienced in these areas, catchments in Cluster 9, Cluster 8, and Cluster 2 have low values of rising limb shape parameters.



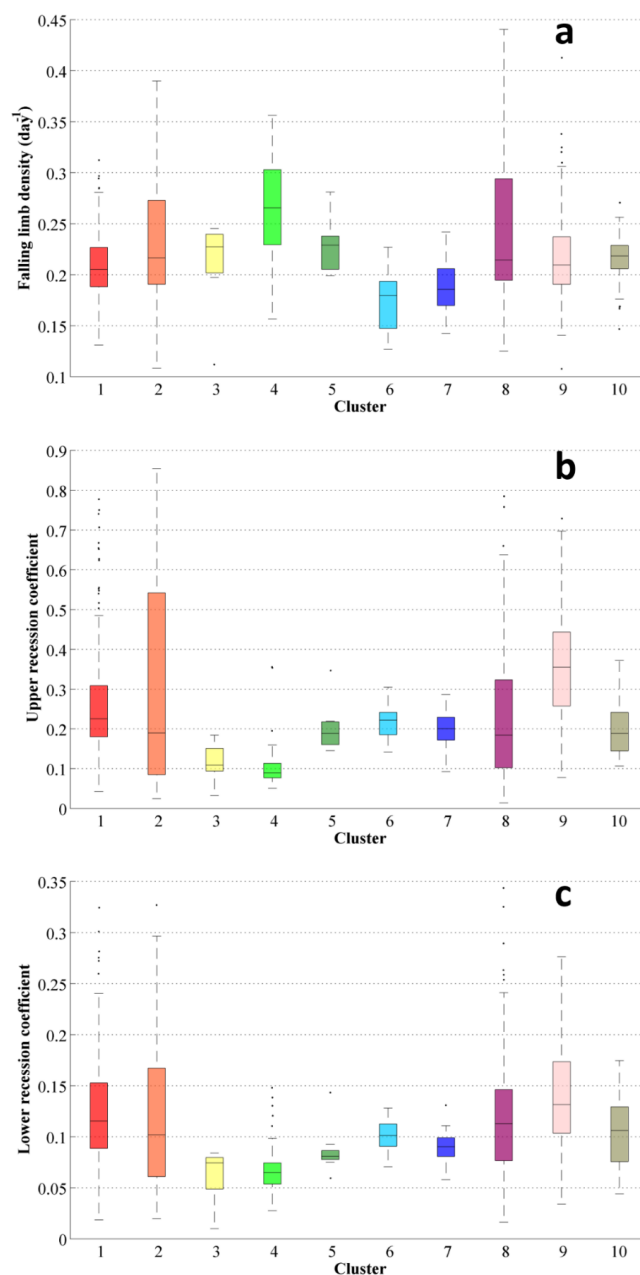
273



274

275 **Figure 7.** Regional variability of streamflow indices associated with the falling limb (a) falling limb density
 276 [day^{-1}], (b) upper recession coefficient, (c) lower recession coefficient over the CONUS. The Great Basin and the
 277 Rocky Mountains, and the High Plains region have high falling limb density. The patterns of the upper recession
 278 coefficient and the lower recession coefficient are similar.

279



280

281 **Figure 8.** Boxplots of the streamflow indices related with the falling limb (a) falling limb density [day⁻¹], (b)
 282 upper recession coefficient, (c) lower recession coefficient of the clusters. Clusters 4, 2, 8 have higher falling limb
 283 densities, while Clusters 6, 7 have lower falling limb densities due to the less forest cover in these arid areas.
 284 Clusters 3, 4, which have a low discharge, have low upper and lower recession coefficients. Clusters 2, 9 have
 285 high recession coefficients due to low slope inclinations.



286

287 6.2 Relation of the Flow Descriptors and the Catchment Attributes

288 The association between the flow descriptors related to rising and falling limbs and catchment attributes is
 289 examined in this section. Table 3 shows the relation of streamflow indices linked with rising limb, and Table 4
 290 shows the association of indices of the falling limb with catchment attributes. Across all five attribute classes, the
 291 vegetation/land cover attributes positively correlate with all rising limb indices (Table 3). It can be seen that the
 292 rising limb density shows a positive correlation with all the three vegetation density indicators, namely fraction
 293 of forest, maximum leaf area index, maximum green vegetation fraction (Table 3).

294

295 However, it is observed that the rising limb scale parameter shows a negative correlation with climate and a
 296 positive association with the vegetation attributes (Table 3). Aridity and frequency of precipitation (Table 3)
 297 display a strong negative association with the rising limb scale parameter. It is noted that the rising limb shape
 298 parameter indicates a positive correlation with vegetation attributes and the fraction of precipitation falling as
 299 snow, mean slope, mean elevation, and sand fraction whereas, it negatively correlates with precipitation
 300 frequency.

301

302 Falling limb density is mainly governed by climate indices and is negatively correlated with the land cover
 303 characteristics (Table 4). Mean elevation also strongly characterizes the nature of the falling limb density. Besides,
 304 aridity and fraction of precipitation falling as snow are also positively correlated with falling limb density.
 305 Recession coefficients are negatively correlated with topographic indices (Table 4). Further, the recession
 306 coefficients show a positive correlation with clay and negative correlations with the fraction of precipitation falling
 307 as snow, forest fraction, and sand fraction. Moreover, the geology attributes such as subsurface porosity reveal a
 308 positive correlation to recession coefficients and a negative with subsurface permeability (Table 4).

309

310

311



Table 3. Correlation between streamflow indices linked with rising limb and the catchment attributes. Green colored coefficients represent positive correlation, and the red-colored correlation coefficients represent the negative correlation. The vegetation/land cover attributes positively correlate with all rising limb indices amongst all five attribute groups. It can be seen that the rising limb density has a positive relationship with all three vegetation density measures. The rising limb scale parameter, has a negative association with climate and a positive relationship with vegetation attributes. The rising limb shape parameter positively correlates with vegetation attributes and the fraction of precipitation that falls as snow, mean slope, mean elevation, and sand fraction.

Spearman rank correlation coefficients	Topography			Climate							Soil			Land cover			Geology		
	Shape parameter	Scale parameter	Rising limb density	Area	Precipitation seasonality	Frac of precp as snow	Aridity	High precp freq	High precp dur	Low precp freq	Low precp dur	Depth to bedrock	Sand frac	Clay frac	Forest frac	LAI maximum	Green veg frac max	Subsurface porosity	Subsurface permeability
				Mean elevation															
				Mean slope															
	-0.17	-0.30		-0.36	-0.33	-0.10	0.08	-0.15			-0.32	-0.28	0.26	0.10	0.20	0.18	-0.16	-0.11	
0.41	-0.13	-0.20		-0.53					-0.63	-0.25	-0.21		-0.15	0.46	0.41	0.44			
0.36	0.35			-0.56															
-0.14																			
0.53																			
-0.16																			
-0.42																			
-0.45																			
-0.29																			
-0.16																			
0.37																			
-0.47																			
0.41																			
0.17																			
0.15																			
-0.16																			



Table 4. Correlation between streamflow indices linked with falling limb and the catchment attributes. Green colored coefficients represent positive correlation, and the red-colored correlation coefficients represent the negative correlation. Climate factors are the principal drivers of falling limb density and are negatively associated with land cover characteristics. Topographic indicators are negatively correlated with recession coefficients. Furthermore, the recession coefficients reveal a positive association with clay and negative correlations with the fraction of precipitation falling as snow, forest fraction, and sand fraction.

Spearman rank correlation coefficients	Topography			Climate							Soil			Land cover			Geology	
	Area	Mean elevation	Mean slope	Precipitation seasonality	Frac of precp as snow	Aridity	High precp freq	High precp dur	Low precp freq	Low precp dur	Depth to bedrock	Sand frac	Clay frac	Forest frac	LAI maximum	Green veg frac max	Subsurface porosity	Subsurface permeability
Falling limb density	-0.13	0.55	0.18		0.42	0.39	0.12	0.12	0.17	0.11	-0.19			-0.17	-0.37	-0.40	-0.08	
Upper recession coefficient		-0.40	-0.38	0.17	-0.46		0.31	-0.11	0.26		0.19	-0.38	0.52	-0.31	-0.09		0.13	-0.09
Lower recession coefficient		-0.35	-0.37	0.22	-0.39		0.27	-0.17	0.19		0.21	-0.23	0.32	-0.28			0.16	-0.18

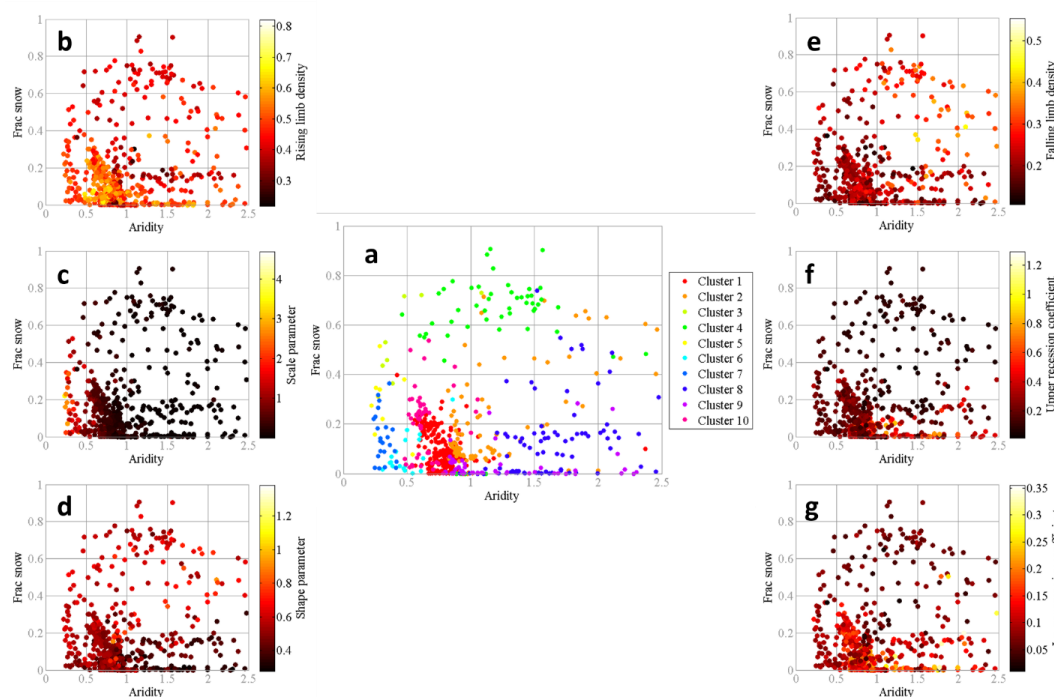


Figure 9. (a) Comparison of the hydrological clusters of Jehn et al. (2020) with the climate index space (fraction of precipitation falling as snow vs. aridity). Single dots show the catchments and are colored by their hydrological clusters. Comparison of the streamflow indices in climate index space (b) rising limb density, (c) rising limb scale parameter, (d) rising limb shape parameter, (e) falling limb density, (f) upper recession coefficient, (g) lower recession coefficient for all catchments. Single dots show the catchments and are colored according to the value of the streamflow indices. Low values of rising limb density, high values of the rising limb shape parameter, and low values of recession coefficients are seen in catchments with a humid environment and a high fraction of precipitation falling as snow. In arid climates with a low fraction of precipitation falling as snow, the lowest values of rising limb scale and shape parameters, as well as the highest values of falling limb density, can be seen.

6.3 Streamflow Indices with Attributes of Climate

Climate attributes seem to be the most important indicator for hydrological behavior in the United States among the various attribute categories (Jehn et al., 2020). Hence, the flow descriptors are then examined in the climate index space (aridity along x-axis and fraction of precipitation falling as snow along the y-axis) to evaluate the main drivers of the catchments. Single dots show the catchments and are colored by their hydrological clusters (Fig. 9.a).

Clusters 5, 6, 7, 1, 10 are characterized by a low fraction of precipitation falling as snow and humid climate, whereas Clusters 3, 4 have humid climate experiencing a high fraction of precipitation falling as snow (Fig. 9.a). Clusters 2, 8, 9 are featured by a low fraction of precipitation falling as snow and arid climate (Fig. 9.a). The three categories mentioned above are referred to as G1, G2, and G3, respectively.



Clusters G1 with a low fraction of precipitation falling as snow with humid climate show (Clusters 1, 9, 10) high rising limb densities (Fig. 9.b) and (Clusters 5, 7) high rising limb scale parameters (Fig. 9.c). This is because the rising limb density negatively correlates with fraction of precipitation falling as snow (Fig. 9.b), whereas the rising limb scale parameter negatively correlates with aridity (Fig. 9.c). Moreover, these Clusters G1 experience a low value of (Clusters 6, 7) falling limb density (Fig. 9.e). This is because the falling limb density positively correlates with the climate indices (Fig. 9.e).

As mentioned earlier, Clusters G2 with humid climate and with a high fraction of precipitation falling as snow (Clusters 3, 4) display low values of rising limb density as rising limb density correlates negatively with the fraction of precipitation falling as snow (Fig. 9.b). G2 witnesses higher values of rising limb shape parameter due to its negative correlation with aridity and positive correlation with the fraction of precipitation falling as snow (Fig. 9.d). Furthermore, the Clusters of G2 (Clusters 3, 4) show low values of recession coefficients as they depict a strong negative correlation with the fraction of precipitation falling as snow (Fig. 9.f, g).

Low values of rising limb scale and shape parameters are noticed for the Clusters 2, 9, 8 (Clusters G3) with arid climate and low fraction of precipitation falling as snow (Fig. 9.c, d) due to its negative correlation with aridity as stated earlier. Cluster 8 experiences the maximum values of falling limb density (Fig. 9.e) where the region witnesses low fraction of snow and arid catchments, due to its strong positive correlates with the aridity.

7 Concluding remarks

Streamflow hydrograph portrays the time distribution of runoff at the point of measurement by a single curve, and the hydrographs are characterized by their time irreversibility property. In this study, the indices related to this characteristic feature are used to study the catchment drivers of streamflow hydrograph. The streamflow indices associated with the time irreversibility of hydrograph open new opportunities to investigate the interaction between topography, soil, climate, vegetation, geology that drive the hydrological behavior of catchments. Moreover, most of the previously presented hydrologic indices are employed only for time-symmetric processes; importance of the time irreversibility of streamflow is highlighted in this study. The indices associated with rising and falling limbs are primarily correlated to distinct catchment attributes, establishing a relationship between the indices and catchment attributes such as climate, topography, soil, geology, and vegetation to delineate the controlling drivers in corresponding hydrograph sections. A set of streamflow indices with temporal asymmetry for 671 catchments in the United States is presented in this study. The regional variations among catchments over the United States are compared and discussed using the spatial maps of streamflow indices. Such spatial maps of the streamflow indices supplement the hydrometeorological time series and catchment attributes provided by Addor et al. (2017).

The study revealed that the rising limb indices such as rising limb density, rising limb shape parameter and rising limb scale parameter correlate positively with vegetation indices. Falling limb density is primarily controlled by climate indices and is negatively correlated with land cover characteristics; the structure of the falling limb density is also closely influenced by mean elevation. Finally, flow descriptors are studied in the climate index space to isolate the runoff generation's leading drivers. High rising limb densities and rising limb scale parameters are observed in catchments with low precipitation falling as snow and a humid climate. It is observed that the catchments with a humid climate and a high fraction of precipitation falling as snow display low values of rising



limb density, high values of the rising limb shape parameter, and low values of recession coefficients. The lowest values of rising limb scale and shape parameters, and the highest values of falling limb density, are seen in catchments of arid climates and a low fraction of precipitation falling as snow.

In general, the contribution of this work lies in differentiating hydrographs depending on their time irreversibility property and using the corresponding indices to provide an alternative methodology for identifying the drivers of streamflow hydrographs. In the context of large sample hydrology research, the concept of time-irreversibility and the indices associated with it could also be used to describe the drivers at catchment scale.

Data availability. The CAMELS dataset can be found at <https://doi.org/10.5194/hess21-5293-2017> (Addor et al. 2017).

Competing interests. The authors declare that they have no conflict of interest.

Acknowledgements. We would like to thank all the people who created the CAMELS dataset. The funding received from the Ministry of Earth Sciences (MoES), Government of India, through the project, “Advanced Research in Hydrology and Knowledge Dissemination”, Project No.: MOES/PAMC/H&C/41/2013-PC-II, is gratefully acknowledged.

References

- Addor, Newman, A. J., Mizukami, N. and Clark, M. P.: The CAMELS data set: catchment attributes and meteorology for large-sample studies, *Hydrol. Earth Syst. Sci.*, 21(10), 5293–5313, doi:10.5194/hess-21-5293-2017, 2017.
- Addor, Nearing, G., Prieto, C., Newman, A. J., Le Vine, N. and Clark, M. P.: A Ranking of Hydrological Signatures Based on Their Predictability in Space, *Water Resour. Res.*, 54(11), 8792–8812, doi:10.1029/2018WR022606, 2018.
- Addor, N., Do, H. X., Alvarez-Garretón, C., Coxon, G., Fowler, K. and Mendoza, P. A.: Large-sample hydrology: recent progress, guidelines for new datasets and grand challenges, *Hydrol. Sci. J.*, 65(5), 712–725, doi:10.1080/02626667.2019.1683182, 2020.
- Alvarez-Garretón, C., Mendoza, P. A., Pablo Boisier, J., Addor, N., Galleguillos, M., Zambrano-Bigiarini, M., Lara, A., Puelma, C., Cortes, G., Garreaud, R., McPhee, J. and Ayala, A.: The CAMELS-CL dataset: Catchment attributes and meteorology for large sample studies-Chile dataset, *Hydrol. Earth Syst. Sci.*, 22(11), 5817–5846, doi:10.5194/hess-22-5817-2018, 2018a.
- Alvarez-Garretón, C., Mendoza, P. A., Boisier, J. P., Addor, N., Galleguillos, M., Zambrano-Bigiarini, M., Lara, A., Puelma, C., Cortes, G., Garreaud, R., McPhee, J. and Ayala, A.: The CAMELS-CL dataset: catchment attributes and meteorology for large sample studies – Chile dataset, *Hydrol. Earth Syst. Sci.*, 22(11), 5817–5846, doi:10.5194/hess-22-5817-2018, 2018b.
- Arsenault, R., Bazile, R., Ouellet Dallaire, C. and Brissette, F.: CANOPEX: A Canadian hydrometeorological watershed database, *Hydrol. Process.*, 30(15), 2734–2736, doi:10.1002/hyp.10880, 2016.



- 435 Berghuijs, W. R., Sivapalan, M., Woods, R. A. and Savenije, H. H. G.: Patterns of similarity of seasonal water
 436 balances: A window into streamflow variability over a range of time scales, *Water Resour. Res.*, 50(7), 5638–
 437 5661, doi:10.1002/2014WR015692, 2014.
- 438 Blöschl, G., Hall, J., Viglione, A., Perdigão, R. A. P., Parajka, J., Merz, B., Lun, D., Arheimer, B., Aronica, G.
 439 T., Bilibashi, A., Boháč, M., Bonacci, O., Borga, M., Čanjevac, I., Castellarin, A., Chirico, G. B., Claps, P.,
 440 Frolova, N., Ganora, D., Gorbachova, L., Gül, A., Hannaford, J., Harrigan, S., Kireeva, M., Kiss, A., Kjeldsen, T.
 441 R., Kohnová, S., Koskela, J. J., Ledvinka, O., Macdonald, N., Mavrova-Guirguinova, M., Mediero, L., Merz, R.,
 442 Molnar, P., Montanari, A., Murphy, C., Osuch, M., Ovcharuk, V., Radevski, I., Salinas, J. L., Sauquet, E., Šraj,
 443 M., Szolgay, J., Volpi, E., Wilson, D., Zaimi, K. and Živković, N.: Changing climate both increases and decreases
 444 European river floods, *Nature*, 573(7772), 108–111, doi:10.1038/s41586-019-1495-6, 2019.
- 445 Clark, M. P., McMillan, H. K., Collins, D. B. G., Kavetski, D. and Woods, R. A.: Hydrological field data from a
 446 modeller’s perspective: Part 2: Process-based evaluation of model hypotheses, *Hydrol. Process.*, 25(4), 523–543,
 447 doi:10.1002/hyp.7902, 2011.
- 448 Coxon, G., Freer, J., Wagener, T., Odoni, N. A. and Clark, M.: Diagnostic evaluation of multiple hypotheses of
 449 hydrological behaviour in a limits-of-acceptability framework for 24 UK catchments, *Hydrol. Process.*, 28(25),
 450 6135–6150, doi:10.1002/hyp.10096, 2014.
- 451 Coxon, G., Addor, N., Bloomfield, J. P., Freer, J., Fry, M., Hannaford, J., Howden, N. J. K., Lane, R., Lewis, M.,
 452 Robinson, E. L., Wagener, T. and Woods, R.: CAMELS-GB: hydrometeorological time series and landscape
 453 attributes for 671 catchments in Great Britain, *Earth Syst. Sci. Data*, 12(4), 2459–2483, doi:10.5194/essd-12-
 454 2459-2020, 2020.
- 455 Do, H. X., Gudmundsson, L., Leonard, M. and Westra, S.: The Global Streamflow Indices and Metadata Archive
 456 (GSIM) – Part 1: The production of a daily streamflow archive and metadata, *Earth Syst. Sci. Data*, 10(2), 765–
 457 785, doi:10.5194/essd-10-765-2018, 2018.
- 458 Duan, Q., Schaake, J., Andréassian, V., Franks, S., Goteti, G., Gupta, H. V., Gusev, Y. M., Habets, F., Hall, A.,
 459 Hay, L., Hogue, T., Huang, M., Leavesley, G., Liang, X., Nasonova, O. N., Noilhan, J., Oudin, L., Sorooshian,
 460 S., Wagener, T. and Wood, E. F.: Model Parameter Estimation Experiment (MOPEX): An overview of science
 461 strategy and major results from the second and third workshops, *J. Hydrol.*, 320(1–2), 3–17,
 462 doi:10.1016/j.jhydrol.2005.07.031, 2006.
- 463 Ehret, U., Gupta, H. V., Sivapalan, M., Weijs, S. V., Schymanski, S. J., Blöschl, G., Gelfan, A. N., Harman, C.,
 464 Kleidon, A., Bogaard, T. A., Wang, D., Wagener, T., Scherer, U., Zehe, E., Bierkens, M. F. P., Di Baldassarre,
 465 G., Parajka, J., van Beek, L. P. H., van Griensven, A., Westhoff, M. C. and Winsemius, H. C.: Advancing
 466 catchment hydrology to deal with predictions under change, *Hydrol. Earth Syst. Sci.*, 18(2), 649–671,
 467 doi:10.5194/hess-18-649-2014, 2014.
- 468 Ghiggi, G., Humphrey, V., Seneviratne, S. I. and Gudmundsson, L.: GRUN: an observation-based global gridded
 469 runoff dataset from 1902 to 2014, *Earth Syst. Sci. Data*, 11(4), 1655–1674, doi:10.5194/essd-11-1655-2019, 2019.
- 470 Gudmundsson, L., Do, H. X., Leonard, M. and Westra, S.: The Global Streamflow Indices and Metadata Archive
 471 (GSIM) – Part 2: Quality control, time-series indices and homogeneity assessment, *Earth Syst. Sci. Data*, 10(2),
 472 787–804, doi:10.5194/essd-10-787-2018, 2018.



- 473 Gupta, H. V., Perrin, C., Blöschl, G., Montanari, A., Kumar, R., Clark, M. and Andréassian, V.: Large-sample
 474 hydrology: a need to balance depth with breadth, *Hydrol. Earth Syst. Sci.*, 18(2), 463–477, doi:10.5194/hess-18-
 475 463-2014, 2014.
- 476 Jehn, F. U., Bestian, K., Breuer, L., Kraft, P. and Houska, T.: Using hydrological and climatic catchment clusters
 477 to explore drivers of catchment behavior, *Hydrol. Earth Syst. Sci.*, 24(3), 1081–1100, doi:10.5194/hess-24-1081-
 478 2020, 2020.
- 479 Koutsoyiannis, D.: Simple stochastic simulation of time irreversible and reversible processes, *Hydrol. Sci. J.*,
 480 doi:10.1080/02626667.2019.1705302, 2020.
- 481 Kuentz, A., Arheimer, B., Hundecha, Y. and Wagener, T.: Understanding hydrologic variability across Europe
 482 through catchment classification, *Hydrol. Earth Syst. Sci.*, 21(6), 2863–2879, doi:10.5194/hess-21-2863-2017,
 483 2017.
- 484 Linke, S., Lehner, B., Ouellet Dallaire, C., Ariwi, J., Grill, G., Anand, M., Beames, P., Burchard-Levine, V.,
 485 Maxwell, S., Moidu, H., Tan, F. and Thieme, M.: Global hydro-environmental sub-basin and river reach
 486 characteristics at high spatial resolution, *Sci. Data*, 6(1), 283, doi:10.1038/s41597-019-0300-6, 2019.
- 487 Mathai and Mujumdar, P. P.: Multisite Daily Streamflow Simulation With Time Irreversibility, *Water Resour.*
 488 *Res.*, 55(11), 9334–9350, doi:10.1029/2019WR025058, 2019.
- 489 McMillan, H. K.: A review of hydrologic signatures and their applications, *WIREs Water*, 8(1), 1–23,
 490 doi:10.1002/wat2.1499, 2021.
- 491 McMillan, H. K., Clark, M. P., Bowden, W. B., Duncan, M. and Woods, R. A.: Hydrological field data from a
 492 modeller’s perspective: Part 1. Diagnostic tests for model structure, *Hydrol. Process.*, 25(4), 511–522,
 493 doi:10.1002/hyp.7841, 2011.
- 494 Newman, A. J., Clark, M. P., Sampson, K., Wood, A., Hay, L. E., Bock, A., Viger, R. J., Blodgett, D., Brekke,
 495 L., Arnold, J. R., Hopson, T. and Duan, Q.: Development of a large-sample watershed-scale hydrometeorological
 496 data set for the contiguous USA: data set characteristics and assessment of regional variability in hydrologic model
 497 performance, *Hydrol. Earth Syst. Sci.*, 19(1), 209–223, doi:10.5194/hess-19-209-2015, 2015.
- 498 Richter, B. D., Baumgartner, J. V., Powell, J. and Braun, D. P.: A Method for Assessing Hydrologic Alteration
 499 within Ecosystems, *Conserv. Biol.*, 10(4), 1163–1174, doi:10.1046/j.1523-1739.1996.10041163.x, 1996.
- 500 Sawicz, K., Wagener, T., Sivapalan, M., Troch, P. A. and Carrillo, G.: Catchment classification : empirical
 501 analysis of hydrologic similarity based on catchment function in the eastern USA, *Hydrol. Earth Syst. Sci.*, 8(3),
 502 2895–2911, doi:10.5194/hess-15-2895-2011, 2011.
- 503 Sawicz, K. A., Kelleher, C., Wagener, T., Troch, P., Sivapalan, M. and Carrillo, G.: Characterizing hydrologic
 504 change through catchment classification, *Hydrol. Earth Syst. Sci.*, 18(1), 273–285, doi:10.5194/hess-18-273-
 505 2014, 2014.
- 506 Serinaldi, F. and Kilsby, C. G.: Irreversibility and complex network behavior of stream flow fluctuations, *Phys.*
 507 *A Stat. Mech. its Appl.*, 450, 585–600, doi:10.1016/j.physa.2016.01.043, 2016.
- 508 Shamir, E., Imam, B., Morin, E., Gupta, H. V. and Sorooshian, S.: The role of hydrograph indices in parameter
 509 estimation of rainfall-runoff models, *Hydrol. Process.*, 19(11), 2187–2207, doi:10.1002/hyp.5676, 2005.



510 Stagge, J. H. and Moglen, G. E.: A nonparametric stochastic method for generating daily climate-adjusted
511 streamflows, *Water Resour. Res.*, 49, 6179–6193, doi:10.1002/wrcr.20448, 2013.
512 Szilagyi, J., Balint, G. and Csik, A.: Hybrid, Markov chain-based model for daily streamflow generation at
513 multiple catchment sites, *J. Hydrol. Eng.*, 11(3), 245–256, 2006.
514
515